NANO LETTERS

pubs.acs.org/NanoLett Letter

Control of Quantized Spontaneous Emission from Single GaAs Quantum Dots Embedded in Huygens' Metasurfaces

Prasad P. Iyer,* Samuel Prescott, Sadhvikas Addamane, Hyunseung Jung, Emma Renteria, Jacob Henshaw, Andrew Mounce, Ting S. Luk, Oleg Mitrofanov, and Igal Brener*

Cite This: https://doi.org/10.1021/acs.nanolett.3c04846 Read Online

ACCESS | Metrics & More | Article Recommendations | Supporting Information

ABSTRACT: Advancements in photonic quantum information systems (QIS) have driven the development of high-brightness, on-demand, and indistinguishable semiconductor epitaxial quantum dots (QDs) as single photon sources. Strain-free, monodisperse, and spatially sparse local-droplet-etched (LDE) QDs have recently been demonstrated as a superior alternative to traditional Stranski−Krastanov QDs. However, integration of LDE QDs into nanophotonic architectures with the ability to scale to many interacting QDs is yet to be demonstrated. We present a potential solution by embedding isolated LDE GaAs QDs within an $Al_{0.4}Ga_{0.6}As$ Huygens' metasurface with spectrally overlapping fundamental electric and magnetic dipolar resonances. We demonstrate for the first time a position- and size-independent, 1 order of magnitude increase in the collection efficiency and emission lifetime control for single-photon emission from LDE QDs embedded within the Huygens' metasurfaces. Our results represent a significant step toward leveraging the advantages of LDE QDs within nanophotonic architectures to meet the scalability demands of photonic QIS.

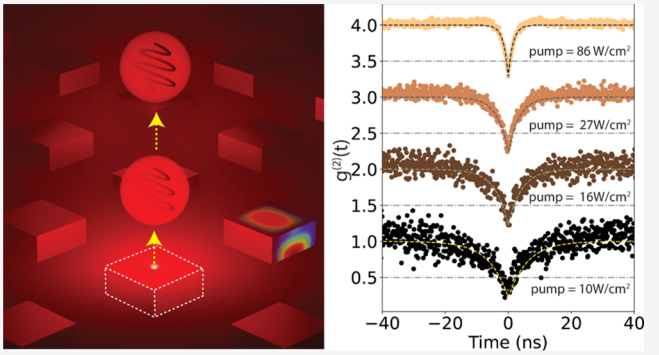

KEYWORDS: *quantum optics, dielectric metasurfaces, single-photon sources, GaAs quantum dot*

Research into on-demand, single and entangled photon sources for all areas of quantum information processing has been actively pursued for the past several decades.[1−4] The development of these sources has evolved in parallel using parametric processes,[5,6] and a variety of single photon emitters[7−11] coupled to engineered photonic structures.[12,13] For the latter type, epitaxial quantum dots (QDs) offer clear advantages, such as wavelength tunable emission,[4] on demand operation,[14] high brightness,[15] high degree of indistinguishability,[16] versatility in entangling photons to other degrees of freedom such as spin,[12,17] and finally, monolithic integration with photonic cavities[18] or other photonic circuits.[19−22] Among epitaxial QDs, local-droplet-etched (LDE) epitaxy QDs are particularly attractive as they form a deeper confinement potential compared to Stranski−Krastanov (S−K) QDs and offer a greater freedom in choosing the dot and host material composition and their areal density, smaller fine structure splitting of the neutral exciton[23] providing a path to wider emission tunability and integration.[24−30]

Alongside improvements in QD epitaxy, we can now leverage recent advancements in nanophotonics to enhance photon collection efficiency,[31,32] control the angular momentum, entangle different degrees of freedom and manipulate interactions between a finite-number of quantum emitters.[33,34] However, the integration of QDs into resonant nanophotonic cavities, which can couple these QDs, is very challenging due to requirements on sub-50 nm scale accurate placement[35] and sub-nm control[36] of the emission wavelength with respect to the cavity resonances.[35] These requirements are critical for scaling up QD sources for quantum information systems (QIS). To overcome the QD limitations, specifically, their random location and size (which defines the emission wavelength), researchers have attempted epitaxial QD growth on nanofabricated wafers[37−42] and fabrication of nanophotonic cavities after determining the location of QDs.[43−46] However, these approaches have limited scalability for a large (>10) number of QDs where only a select few emitters on a wafer are enhanced by the nanophotonic design. Here, we demonstrate that semiconductor metasurfaces with embedded LDE QDs can form a potential solution to overcome the randomness of QD localization inherent to the epitaxial growth process while taking advantage of the greater monodispersity, brightness and sparsity of these QDs.[26] The metasurfaces offer an attractive

Received: December 10, 2023
Revised: March 27, 2024
Accepted: April 1, 2024

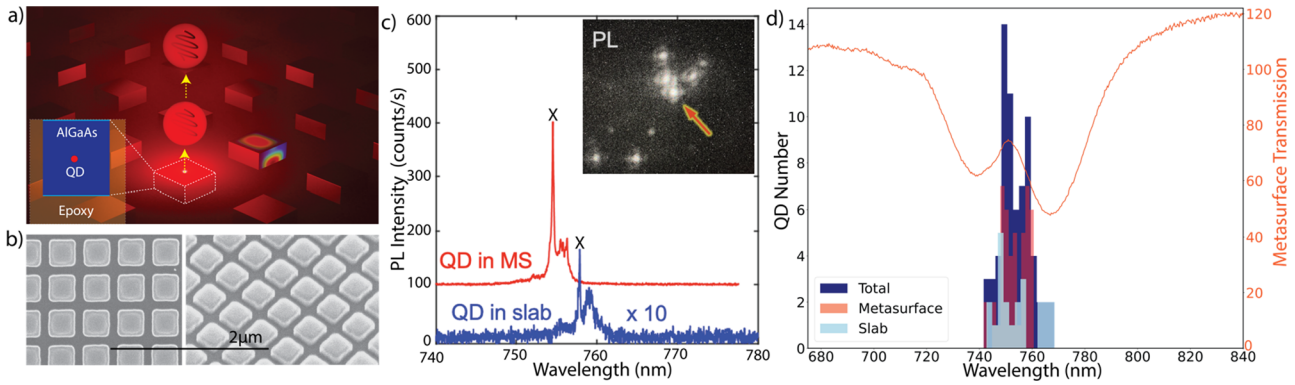

Figure 1. Photoluminescence enhancement with Mie metasurfaces. (a) Illustration of Huygens' metasurface (MS) made of AlGaAs resonators with an embedded GaAs quantum dot (QD). The color-maps on the resonators' top and side surfaces show the normalized electric field profiles (min−blue, max−red) of optical resonances. (b) Scanning electron microscopy (SEM) images of fabricated metasurfaces with top (left) and tilted (right) views. These images were taken prior to the flip-chip bonding step. (c) Photoluminescence (PL) spectra of GaAs LDE QDs from a Huygens' metasurface and from a uniform epitaxial layer (slab) demonstrating an order of magnitude increase of PL emission into free space. The inset shows a microscope PL image where individual QDs within the metasurface can be seen. (d) Distribution of QD exciton (X) emission wavelength for 80 randomly selected LDE GaAs QDs within the metasurface (red), the slab (light blue), and the total (dark blue). The center of this narrow distribution (< ±5 nm) is aligned with the Huygens' point for selected metasurface, identified as a local peak at 750 nm in the metasurface transmission spectrum (orange curve).

platform where a single design can enhance the emission properties of all the LDE QDs grown on the wafer regardless of their size and position.[47−51] Furthermore, the monolithic integration of LDE QDs into the metasurface offers a robust semiconductor platform for scientific exploration and future applications. We demonstrate that $Al_{0.4}Ga_{0.6}As$ Huygens' metasurfaces provide an average of 10× enhancement of the collected photoluminescence (PL) from the embedded single LDE QDs when compared with QDs in an unpatterned region. The enhanced efficiency enables single-photon spectroscopy of excitonic species in LDE QDs with excitation power densities over an order of magnitude lower than the same QDs present in unpatterned thin films. Surprisingly, we discovered that, at the low CW-pump power densities incident on the metasurface (<10W/cm^2, 515 nm), the effective lifetime of single photon emitters can be dynamically controlled by nearly an order of magnitude (8−1 ns) with the pump power. Ultimately, a metasurface with embedded high brightness LDE QDs could provide an efficient route toward realizing scalable-coupled quantum meta-atoms suitable for quantum information processing, and communications.[52−54]

A Huygens' metasurface forms an ideal platform for embedding isolated semiconductor QDs because of spatial uniformity of modes within individual resonators, created by overlapping the fundamental electric and magnetic dipolar (ED and MD) resonances.[50,55] This spatial uniformity of the resonant fields (Figure 1a, See Supporting Information (SI) Figures S6−S8) minimizes the effect of random positioning of the QD within the resonator.[56] Additionally, the broadband spectral response of the overlapping dipolar resonances covers the wavelength distribution of the QD emitters grown on the wafer. $Al_{0.4}Ga_{0.6}As$ is a suitable host for GaAs LDE QDs because of the larger bandgap ($E_g \sim 2.039$ eV or 607.8 nm at 15K[57]) and high refractive index ($n = 3.43$[58]) required to form resonant semiconductor metasurfaces. The modal dispersion of the fundamental electric and magnetic dipolar modes can be engineered by controlling the geometry (width, sub-wavelength pitch, and height) of the $Al_{0.4}Ga_{0.6}As$ resonators.

$Al_{0.4}Ga_{0.6}As$ thin films with embedded GaAs LDE QDs were epitaxially grown (see Methods) and fabricated into metasurface resonators. We used a flip-chip process (see Methods) to eliminate the influence of the high index absorbing GaAs substrate on embedded QD emitters (Figure 1b).[5] In this process, we leverage the precise control of the QDs' vertical positioning within the resonators provided by the epitaxial growth. Figure 1c shows that the PL peak intensity (measured at 15 ± 5 K) from an isolated GaAs LDE QD embedded within an exemplar Huygens' metasurface is enhanced by an order of magnitude when compared to the QD emission from an unpatterned slab. Furthermore, the PL image (inset in Figure 1c) demonstrates that the emission enhancement from the QDs (surviving the nanofabrication process) is agnostic of the position of the QDs within the metasurface. Interestingly, the distribution of emission wavelength for the QDs present on the wafer (both within the metasurface and within the unpatterned region) overlaps well with the spectral band where the metasurface supports the fundamental electric and magnetic dipolar resonances (see SI). The band, centered at 745 nm, manifests itself as a local maximum in the metasurface transmission spectrum (Figure 1d). This spectral overlap specifically highlights the capability of the low-Q modes to enhance the QD emission regardless of the size distribution gained during the LDE growth process. The position- and emission wavelength-agnostic enhancement of isolated LDE GaAs QDs show the potential for Huygens' metasurfaces not only as a characterization platform of novel QDs but also as a platform to engineer the interactions between isolated QDs through resonant near-field interactions.

To evaluate the effect of the metasurface modes on the PL, we collected spectra of several QDs embedded into three metasurfaces of different designs (Figure 2a−c) and compared them to PL from QDs embedded in a uniform layer of $Al_{0.4}Ga_{0.6}As$ (referred to here as the slab) (see Methods for details). Figure 2d−f summarize the peak PL intensity and the central wavelength of emission for the tested single QDs. For MS1 and MS3 with the ED and MD modes overlapping with the wavelength of the QD emission (Figure 2a,c), the average PL intensity is higher by a factor of ∼10 in comparison to the average emission from QDs embedded in the slab (Figure 2d,f). In contrast, MS2 with the ED and MD modes at ∼825

https://doi.org/10.1021/acs.nanolett.3c04846
Nano Lett. XXXX, XXX, XXX−XXX

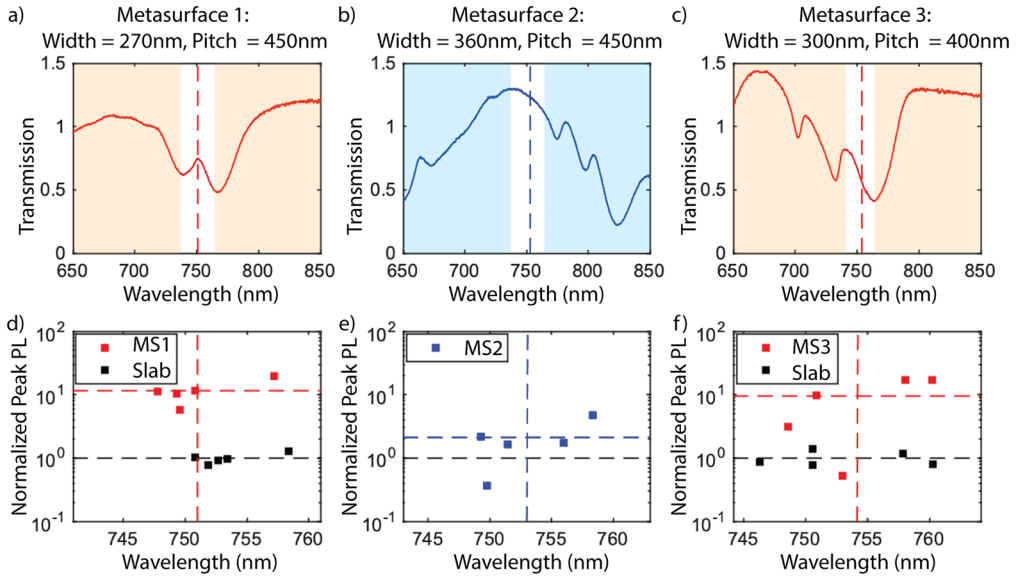

Figure 2. Metasurface optical properties and corresponding QD PL emission enhancement. (a−c) Transmission spectra of three metasurfaces (MS) of different geometry (resonator width and pitch). The spectra are normalized to transmission through the substrate. The Mie modes are aligned with the QD emission wavelength for MS1 and MS3, and red-shifted by more than 50 nm for MS2. The white region between the shaded region in panels a−c represents the wavelengths plotted in panels d−f, respectively. (d−f) PL peak intensity for the dominant exciton transition from 5 randomly selected QDs within MS1, MS2, and MS3, and form QDs located in the unpatterned slab. PL intensity for every QD is normalized to the average peak intensity of QD PL from the slab. Dashed lines mark the average values for each MS.

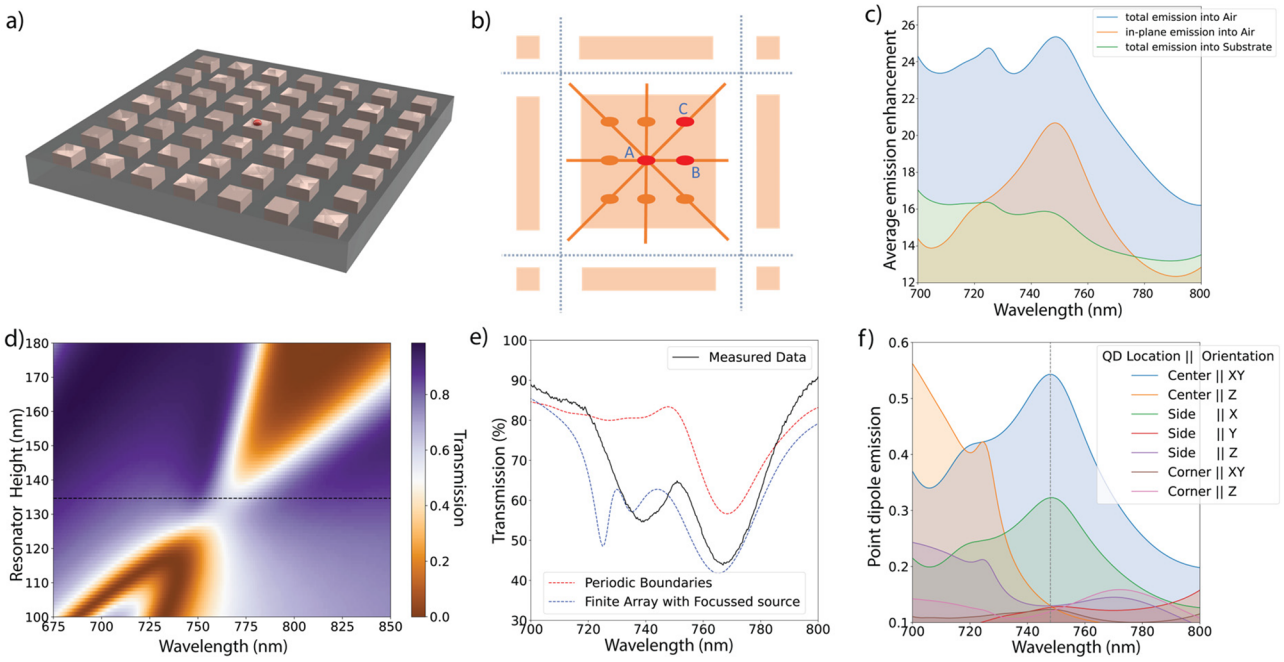

Figure 3. Full wave simulation of emission from Mie metasurfaces. (a) Illustration of a finite array (7 × 7) of resonators with a QD in the central resonator used in the FDTD simulations. (b) Schematic representing 9 simulated positions of the QD within the resonator. Red dots show the three unique locations (Center − A, Side − B, and Corner − C). (c) Average emission enhancement for a point dipole embedded within the metasurface resonator (blue, total dipole emission into air, orange, − in-plane dipole emission into air, and green, − total dipole emissioninto substrate) with respect to the same source embedded into an unpatterned slab. (d) Metasurface transmission map showing the dispersion of the electric (ED) and magnetic (MD) dipolar modes for a varying resonator height. The ED and MD modes overlap to form the Huygens' metasurface for h = 135 nm (marked by the horizontal dashed line) at a height of 135 nm. (e) Full wave simulation of the transmission spectrum (dashed blue line) and the experimentally measured transmission spectrum of the Huygens' metasurface (black line) using weakly focused (NA = 0.15) incident light. A simulated spectrum for periodic boundary conditions is shown by a red line for comparison. (f) Emission spectra of the point dipole source placed at positions A, B, and C with different dipole moment orientations (x,y − in plane and z − out of plane). Emission efficiency peaks at ∼750 nm for the QD placed at the center (blue line) and side (green) locations for the x-oriented dipole.

nm (Figure 2b), outside the region of QD PL emission, shows only marginal enhancement (∼2) (Figure 2e). From these results and assuming that the photonic environment does not affect the emission rate appreciably (see SI), we conclude that

https://doi.org/10.1021/acs.nanolett.3c04846
Nano Lett. XXXX, XXX, XXX−XXX

the ED and MD modes aligned with the QD emission wavelength yield a 1 order of magnitude increase in the number of out-coupled photons. Furthermore, our metasurface fabrication process does not deteriorate the QD emission properties.

To reveal the underlying mechanisms that lead to the observed enhancement of photon emission, we evaluated the effect of the metasurface on coupling the emission from QDs into free space using numerical electromagnetic simulations. We modeled a QD emitter as a point source of electromagnetic radiation placed inside the metasurfaces. It is important to note that due to a relatively low density of QDs (~0.1 μm^{-2}), we can assume that a Mie resonator with a dot is surrounded by resonators without dots. Therefore, the commonly used periodic boundary conditions[50] do not represent a realistic system. Thus, we chose to model a larger area metasurface. Furthermore, the lateral position of the QD within the resonator and the orientation of the QD dipole moment are both random. To evaluate a realistic effect of the metasurface on the QD emission, we positioned a Mie resonator with a point source emitter in the center of a 9 × 9 array of passive resonators (as illustrated in Figure 3a). We then simulated the light emission from the point source positioned in 9 different locations within the central resonator (Figure 3b) and with three primary orientations of the dipole moment (x, y, and z). The full set of positions and dipole moment orientations represents 27 equally probable cases of single QDs embedded in the Mie resonator (assuming that all of the dipole orientations are equally probable; see SI for simulation details). To quantify the metasurface effect, we compared the QD emission spectrum for the metasurface (averaged over the 27 cases) to that for an $Al_{0.4}Ga_{0.6}As$ slab with embedded QDs. A normalized spectrum of the QD emission from the metasurface is shown in Figure 3c. The emission enhancement factor has a peak value of ~25 at exactly the wavelength at which the ED and MD modes overlap (~750 nm, Figure 3d,e). We note that the simulations show enhancement for emission both into the air and into the sapphire substrate. However, for this metasurface design and at this wavelength, the enhancement factor for emission into air is higher in comparison to the emission into the substrate (a factor of ~16).

The spectrum in Figure 3c shows that the QD emission is enhanced not only at ~750 nm but also within a wide band with a complex spectral structure. The source of this structure is revealed in Figure 3f by plotting enhancement spectra for individual dipole moment orientations and QD positions within the resonator. This decomposition of the overall enhancement allowed us to correlate the main enhancement peak with specific locations and dipole orientations of the point emitter. The main peak at 750 nm is undoubtedly caused by the ED mode coupled to a QD positioned at the center of the resonator with the dipole moment in the metasurface plane (point A in Figure 3b). A QD shifted halfway to the side (point B) also shows a main peak at 750 nm, albeit with reduced enhancement. These two positions/orientations are expected to couple most efficiently to the ED mode due to the spatial overlap with the ED mode profile. We therefore conclude that the observed emission enhancement at 750 nm can be assigned primarily to spatial and spectral overlap of the ED mode with the QD emission. Other modes, including the MD mode, which is expected to be excited most efficiently by a QD positioned at Point C and having the dipole moment along the z-axis, also contribute to the overall enhancement, however, at a lower level (less than 20% relative to ED).

The numerical model of the QD embedded in the metasurface allows us to quantify the fraction of total number of photons emitted into air, the substrate, and into the metasurface layer and compare the emission pattern to that of a QD embedded in an $Al_{0.4}Ga_{0.6}As$ slab. A table below shows a distribution of emitted photons between the air, substrate, and the metasurface layer for a QD positioned in the middle of the central resonator and photons polarized in the metasurface plane (λ = 750 nm). (See Supporting Information Figure S9 for the radiation patterns.) The metasurface facilitates the out-coupling of emitted photons into air (~35%; Table 1). In contrast, less than 2% of photons couple into air for a QD placed in an $Al_{0.4}Ga_{0.6}As$ slab.

Table 1. Emission Profile of In-Plane Polarized Photons from an Embedded Quantum Dot at 750 nm

Region	AlGaAs slab (%)	Metasurface (%)
Air	1.7	**35**
Slab/Metasurface	**93.5**	6
Substrate	4.8	59

To evaluate the potential of QDs embedded in the Huygens' metasurfaces as single-photon sources, we analyzed single-photon emission from isolated QDs and its dependence on optical pump intensity for non-resonant continuous wave (CW) excitation at 515 nm. First, we characterized the PL saturation characteristics of a representative QD within the metasurface by measuring the PL spectrum dependence on the pump intensity. At low intensities (<100 W/cm^2), we observed a narrow (resolution-limited) QD spectrum, which broadens as the pump power is increased. Spectrum broadening has been observed previously in QDs at high intensities of excitation, and it has been attributed to carrier accumulation near the dot under excitation.[59−62] In addition to the broadening, we observed that the photon emission rate for the dominant QD transition (at 761 nm) started saturating above ~180 W/cm^2 of excitation intensity. A similar saturation behavior occurred for a representative QD within the slab, albeit at a slightly higher intensity (~280 W/cm^2) (see SI). We then performed second order autocorrelation statistics measurements ($g^{(2)}(t)$) in the low excitation intensity regime using a Hanbury−Brown−Twiss (HBT) interferometer (see Methods). We measured $g^{(2)}(0) \sim 0.2-0.3$ for a pumping power of ~10 W/cm^2 (Figure 4b). We note that this result is achieved without the use of narrow (sub-GHz) spectral filters.[27]

The $g^{(2)}(t)$ traces (Figure 4b) show that the QD excitation lifetime increases at low pumping powers. For quantitative analysis, the measured $g^{(2)}(t)$ traces at each pump power were fitted using the equation $g^{(2)}(t) = 1 - ae^{-|t|/\tau}$, following the procedure in refs 63−65. Here a represents the purity of the single photon source such that $a = 1 - g^{(2)}(t = 0)$ and τ represents the lifetime of the QD. We discovered that the effective lifetime of the single-photon emission from LDE QDs varies by nearly an order of magnitude: under very low excitation intensity (10 W/cm^2), we observed a lifetime of 6.0 ± 1 ns. It decreases by almost an order of magnitude (1.0 ± 0.34 ns) as we increased the intensity to 85W/cm^2 (Figure 4c). By tracking the photon emission rate ($1/\tau$) as a function of the optical pump power we found a linear trend which when

https://doi.org/10.1021/acs.nanolett.3c04846
Nano Lett. XXXX, XXX, XXX−XXX

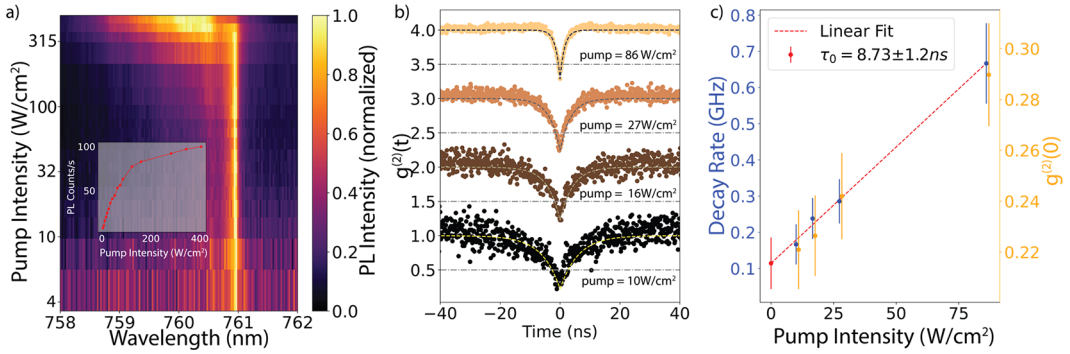

Figure 4. Single-photon characteristics of an isolated QD. (a) Map of PL spectra from a single QD within the metasurface under continuous wave (CW) pumping at 515 nm (spectra are normalized for each pump power). The CW pump power increases along the vertical axis (log-scale). The bright streak at 760.9 nm represents the X transition of the QD that undergoes spectral broadening under high pump powers. Inset: Peak PL intensity was as a function of the pump power. The QD emission exhibits saturation after 100 W/cm^2 of focused illumination. (b) Waterfall style plot of the photon autocorrelation function from the same single QD under varying pump powers (10−86 W/cm^2). The dashed lines represent the single exponential fits to the rising edge of the $g^{(2)}(t)$ plots. (c) QD decay rate (left axis, blue dots) as a function of the pump power. The rate values are extracted from fitting the $g^{(2)}(t)$ traces in (b). (dashed lines). The red dashed line represents a linear fit to the blue dots. Extrapolation of the linear fit to zero pump power gives an intrinsic QD exciton lifetime of 8.73 ± 1.2 ns (red dot). The anti-bunching dip at t = 0 is plotted in orange on the right axis to demonstrate that the QD behaves like a single-photon source under these pump powers.

extrapolated to zero yielded an intrinsic lifetime of the QD-metasurface system of 8.73 ± 1.2 ns (Figure 4c).

This intrinsic lifetime for the GaAs LDE QDs-metasurface system (while operating as a single photon source) is surprising. First of all, the intrinsic lifetime of GaAs LDE QDs has been previously estimated to be less than 400 ps.[66−68] Second, nanopatterning of light-emitters typically reduces the effective lifetime due to the increase of surface-related defect states.[18,47,51,69] In contrast, here both dots embedded in the metasurface and in the slab (see SI) show longer lifetimes than previously reported in the literature. This indicates that the metasurface fabrication process—including the nanoscale dry etching—has not degraded the QD emission properties.

In previous demonstrations of controlling the emission lifetime of a single QD (for example performed with an InAs SK QD coupled to a microdisk cavity), a large difference in the lifetime between the QDs in the cavity and in an unpatterned region was attributed (tentatively) to Purcell suppression.[64] However, FDTD simulations (matching experimental spectra) indicate that the Purcell factor for emitters embedded into the Mie resonator is on average close to 1 (SI), suggesting that we are not extending the lifetime through Purcell suppression of emission. Furthermore, the lifetime estimates derived from the $g^{(2)}(t)$ measurements give an effective performance of the QD-metasurface system that cannot be attributed solely to the intrinsic lifetime of the GaAs QDs. The pump excites charge carriers in both the GaAs QD and the $Al_{0.4}Ga_{0.6}As$ resonator. Hence, the effective lifetime of the QD emission could result from two pathways—namely, direct excitation of the carriers in the QD and capture of carriers excited in the AlGaAs resonator. Previous non-resonant excitation of the GaAs LDE QDs yielded extended lifetimes beyond 500 ps suggesting the possibility of a charge reservoir in the barrier $Al_{0.4}Ga_{0.6}As$ layer.[66] Additional experiments varying the optical pump wavelength from 515 nm to the emission wavelength at 761 nm need to be performed to identify the source of the lifetime increase. Ultimately, we have identified that the effective lifetime of the embedded QD can be varied by 1 order of magnitude by varying the optical pump power.

In conclusion, we have demonstrated an order of magnitude enhancement in emission intensity for LDE GaAs QDs embedded within a Huygens' metasurface independent of the QD placement with respect to the Mie resonator and the QD emission wavelength. We have developed a combination of novel monolithic QD growth, nanophotonic design, and nanofabrication, which enabled us to collect the emission from an isolated QD embedded within the metasurface. We have demonstrated that overlapping the fundamental dipolar Mie modes with the emission wavelength of the QDs results in the observed enhancement, with the electric dipolar mode providing the main contribution, while the Purcell factor remains close to 1. Furthermore, we were able to control the lifetime of the metasurface-embedded QDs by an order of magnitude by varying the optical pump power. The monolithic semiconductor architecture demonstrated here could offer an ideal platform for characterization and calibration of the embedded LDE QDs whose emission could be tuned through the epitaxial growth and enhanced by the Huygens's metasurface geometry over the visible and near-infrared wavelengths. We expect that the combination of semiconductor metasurfaces with embedded LDE QD emitters will facilitate unexplored multiple quantum emitter phenomena with the potential for novel quantum sensing and communication technologies.[1,52]

METHODS

Epitaxial Growth. The sample described in this study is grown using molecular beam epitaxy (MBE) on a semi-insulating GaAs (100) substrate (VA1166). The native oxide on the substrate is first thermally desorbed in situ at 630 °C for 10 min. The growth of the epilayers is then initiated at a substrate temperature of 600 °C. The structure mainly consists of a 300 nm GaAs buffer, followed by a 500 nm $Al_{0.75}Ga_{0.25}As$ etch-stop layer and a 140 nm thick $Al_{0.4}Ga_{0.6}As$ layer. The latter layer is embedded with LDE GaAs QDs (in the middle—at 70 nm) and is protected on both top (from air) and bottom (from the etch stop layer) sides with 5 nm GaAs layers (see SI). For the QD layer, the growth process is paused in the middle of the $Al_{0.4}Ga_{0.6}As$ barrier layer, and the substrate temperature is increased to 620 °C under an arsenic soak. The excess arsenic on the surface is removed by annealing the substrate at this temperature for 40 s without any arsenic

https://doi.org/10.1021/acs.nanolett.3c04846
Nano Lett. XXXX, XXX, XXX−XXX

supply. Next, only aluminum is introduced to form droplets with a nominal thickness of 0.6 ML. The arsenic supply is now opened, and the droplets are annealed in a low-arsenic environment for 300 s to promote etching of nanovoids. To form QDs, GaAs is deposited using migration-enhanced epitaxy (MEE) to ensure large diffusion lengths and preferred nucleation inside the nanovoids. This consists of alternate deposition of Ga (0.5 s) and As (10 s) to get a total GaAs QD thickness of 1.75 nm (24 loops). The QDs are finally annealed for 300 s before going back to growing the rest of the $Al_{0.4}Ga_{0.6}As$ membrane layer. The Ga and Al growth rates are 0.52 and 0.34 ML/s, respectively, for the QD layer. The As:Ga beam equivalent pressure ratio was maintained at 15 for most of the growth and reduced to ∼7.5 for a low-arsenic environment. The substrate temperature is measured using a pyrometer. The growth rates are calibrated on a GaAs substrate using reflection high-energy electron diffraction (RHEED).

Fabrication. To define the metasurfaces on the wafer, a PMMA 495/950 A2 dual-layered e-beam resist was coated (3000 rpm for 30 s) and baked at 180 °C for 1 min, 30 s. The metasurfaces were patterned using the e-beam lithography process (600 $\mu C/cm^2$, 100 kV) and developed with MIBK/IPA for 60 s. The samples were then dry-etched by the reactive ion etching (RIE) process in a mixture of BCl_3, Cl_2, Ar, and N_2 gases (10, 10, 10, and 3.5 cm^3/min, respectively). After defining the AlGaAs metasurface, the remaining e-beam resist from the metasurface is removed with Remover PG at 75 °C for 20 min. The sample is then flip-chip-bonded onto sapphire substrates using epoxy (353ND, EPO-TEK). The GaAs substrate was then removed by using mechanical lapping and wet-etching processes. In the wet-etching process, an ammonium hydroxide solution ($NH_4OH:H_2O_2$ 1:33) was used to etch the remaining GaAs substrate and spacer in a customized jet etcher. Then, hydrochloric acid (HCl) was used to remove the $Al_{0.55}Ga_{0.45}As$ etch-stop layer. Finally, only the QD metasurface remained on the sapphire substrate.

Photoluminescence and $g^{(2)}(t)$ Measurement Setup. The fabricated samples containing QDs integrated into metasurfaces and into the $Al_{0.4}Ga_{0.6}As$ slab were characterized at $T = 15 \pm 5$ K using an optical cryostat. A wide-field microscopy configuration and a CCD camera were used to locate the QDs within the sample. Then, individual QDs were illuminated in a confocal microscopy configuration using a tightly focused beam from a fiber-coupled 515 nm laser diode running below the lasing threshold. Photoluminescence from individual QDs was collected using a 50× microscope objective (NA = 0.42) and analyzed with a 1200 g/mm grating spectrometer. Two long-pass filters were used to block the excitation beam light from the laser. The same optical setup was used for the optical excitation power dependence experiments (Figure 4a) and for $g^{(2)}(t)$—correlation function measurements. Two angle-tunable edge filters (short-pass and long-pass) were added to the setup for these measurements to isolate emission due to the main optical transition in the QD. $g^{(2)}(t) = \frac{\langle n_1(t)n_2(t)\rangle}{\langle n_1(t)\rangle\langle n_2(t)\rangle}$ was estimated by counting the number of photons in each of the two ($n_{1,2}(t)$) superconducting nanowire broadband detectors as a function of time t.

Transmission Measurement Setup. The transmission spectra through the metasurface were measured using a white light (Tungsten Halogen lamp) source and visible spectrometer (Ocean Optics, Jazz) and two 50 mm Plano-convex lenses above and below the metasurface. The spectra measured through the metasurface was normalized to the transmission through an adjacent region on the sample without the metasurface, containing only the sapphire substrate. The dark counts on the spectrometer were subtracted from both (metasurface and background) spectra prior to normalization.

■ ASSOCIATED CONTENT

Supporting Information

The Supporting Information is available free of charge at https://pubs.acs.org/doi/10.1021/acs.nanolett.3c04846.

Additional details regarding the experimental setup, simulation details including mode profiles etc. (PDF)

■ AUTHOR INFORMATION

Corresponding Authors

Prasad P. Iyer − *Center for Integrated Nanotechnologies, Sandia National Lab, Albuquerque, New Mexico 87185, United States; Sandia National Laboratories, Albuquerque, New Mexico 87185, United States;* orcid.org/0000-0002-6898-3619; Email: ppadma@sandia.gov

Igal Brener − *Center for Integrated Nanotechnologies, Sandia National Lab, Albuquerque, New Mexico 87185, United States; Sandia National Laboratories, Albuquerque, New Mexico 87185, United States;* orcid.org/0000-0002-2139-5182; Email: ibrener@sandia.gov

Authors

Samuel Prescott − *University College London, Electronic and Electrical Engineering, London WC1E 7JE, U.K.;* orcid.org/0009-0003-5256-3075

Sadhvikas Addamane − *Center for Integrated Nanotechnologies, Sandia National Lab, Albuquerque, New Mexico 87185, United States; Sandia National Laboratories, Albuquerque, New Mexico 87185, United States*

Hyunseung Jung − *Center for Integrated Nanotechnologies, Sandia National Lab, Albuquerque, New Mexico 87185, United States; Sandia National Laboratories, Albuquerque, New Mexico 87185, United States;* orcid.org/0000-0002-3925-3238

Emma Renteria − *Center for High Technology Materials, University of New Mexico, Albuquerque, New Mexico 87185, United States*

Jacob Henshaw − *Center for Integrated Nanotechnologies, Sandia National Lab, Albuquerque, New Mexico 87185, United States; Sandia National Laboratories, Albuquerque, New Mexico 87185, United States*

Andrew Mounce − *Center for Integrated Nanotechnologies, Sandia National Lab, Albuquerque, New Mexico 87185, United States; Sandia National Laboratories, Albuquerque, New Mexico 87185, United States*

Ting S. Luk − *Center for Integrated Nanotechnologies, Sandia National Lab, Albuquerque, New Mexico 87185, United States; Sandia National Laboratories, Albuquerque, New Mexico 87185, United States*

Oleg Mitrofanov − *University College London, Electronic and Electrical Engineering, London WC1E 7JE, U.K.;* orcid.org/0000-0003-3510-2675

Complete contact information is available at: https://pubs.acs.org/10.1021/acs.nanolett.3c04846

https://doi.org/10.1021/acs.nanolett.3c04846
Nano Lett. XXXX, XXX, XXX−XXX

Author Contributions

P.P.I., O.M., T.S.L., and I.B. designed the study. P.P.I. and S.P. performed the numerical electromagnetic simulations. P.P.I., H.J., and E.R. fabricated the device. S.A. grew the support wafer in MBE. P.P.I., O.M., and T.S.L. measured the quantum dot PL and transmission spectra. P.P.I., J.H., and A.M. performed the $g^{(2)}(t)$ measurements. The manuscript was written with inputs from all the authors.

Funding

U.S. Department of Energy (BES20017574). S.P. was supported by the EPSRC (EP/S022139/1).

Notes

The authors declare no competing financial interest.

■ ACKNOWLEDGMENTS

This work was supported by the U.S. Department of Energy, Office of Basic Energy Sciences, Division of Materials Sciences and Engineering and performed, in part, at the Center for Integrated Nanotechnologies, an Office of Science User Facility operated for the U.S. Department of Energy (DOE) Office of Science. Sandia National Laboratories is a multimission laboratory managed and operated by National Technology and Engineering Solutions of Sandia, LLC, a wholly owned subsidiary of Honeywell International, Inc., for the U.S. Department of Energy's National Nuclear Security Administration under contract DE-NA0003525. This paper describes objective technical results and analysis. Any subjective views or opinions that might be expressed in the paper do not necessarily represent the views of the U.S. Department of Energy or the United States Government. Part of this work was enabled by the use of pyscan (github.com/sandialabs/pyscan), software made available by the Center for Integrated Nanotechnologies, which is an Office of Science User Facility operated for the U.S. Department of Energy.

■ REFERENCES

(1) Heindel, T.; Kim, J.-H.; Gregersen, N.; Rastelli, A.; Reitzenstein, S. Quantum dots for photonic quantum information technology. *Advances in Optics and Photonics* **2023**, *15* (3), 613−738.

(2) Wang, H.; Qin, J.; Ding, X.; Chen, M.-C.; Chen, S.; You, X.; He, Y.-M.; Jiang, X.; You, L.; Wang, Z. Boson sampling with 20 input photons and a 60-mode interferometer in a 1 0 14-dimensional hilbert space. *Physical review letters* **2019**, *123* (25), 250503.

(3) Senellart, P.; Solomon, G.; White, A. High-performance semiconductor quantum-dot single-photon sources. *Nat. Nanotechnol* **2017**, *12* (11), 1026−1039.

(4) Uppu, R.; Pedersen, F. T.; Wang, Y.; Olesen, C. T.; Papon, C.; Zhou, X.; Midolo, L.; Scholz, S.; Wieck, A. D.; Ludwig, A.; Lodahl, P. Scalable integrated single-photon source. *Science advances* **2020**, *6* (50), No. eabc8268.

(5) Santiago-Cruz, T.; Gennaro, S. D.; Mitrofanov, O.; Addamane, S.; Reno, J.; Brener, I.; Chekhova, M. V. Resonant metasurfaces for generating complex quantum states. *Science* **2022**, *377* (6609), 991−995.

(6) Santiago-Cruz, T. s.; Fedotova, A.; Sultanov, V.; Weissflog, M. A.; Arslan, D.; Younesi, M.; Pertsch, T.; Staude, I.; Setzpfandt, F.; Chekhova, M. Photon Pairs from Resonant Metasurfaces. *Nano Lett.* **2021**, *21* (10), 4423−4429 (pmid = 33971095, pmcid = PMC8289292).

(7) Lukin, D. M.; Guidry, M. A.; Yang, J.; Ghezellou, M.; Mishra, S. D.; Abe, H.; Ohshima, T.; Ul-Hassan, J.; Vučković, J. Optical superradiance of a pair of color centers in an integrated silicon-carbide-on-insulator microresonator. *arXiv preprint arXiv:2202.04845* **2022**, DOI: 10.48550/arXiv.2202.04845.

(8) Higginbottom, D. B.; Kurkjian, A. T.; Chartrand, C.; Kazemi, M.; Brunelle, N. A.; MacQuarrie, E. R.; Klein, J. R.; Lee-Hone, N. R.; Stacho, J.; Ruether, M. Optical observation of single spins in silicon. *Nature* **2022**, *607* (7918), 266−270.

(9) Senichev, A.; Martin, Z. O.; Peana, S.; Sychev, D.; Xu, X.; Lagutchev, A. S.; Boltasseva, A.; Shalaev, V. M. Room-temperature single-photon emitters in silicon nitride. *Science Advances* **2021**, *7* (50), No. eabj0627.

(10) Lukin, D. M.; Guidry, M. A.; Vučković, J. Integrated quantum photonics with silicon carbide: challenges and prospects. *PRX Quantum* **2020**, *1* (2), 020102.

(11) Zhang, G.; Cheng, Y.; Chou, J.-P.; Gali, A. Material platforms for defect qubits and single-photon emitters. *Applied Physics Reviews* **2020**, *7* (3), 031308.

(12) Atatüre, M.; Englund, D.; Vamivakas, N.; Lee, S.-Y.; Wrachtrup, J. Material platforms for spin-based photonic quantum technologies. *Nat. Rev. Mater.* **2018**, *3* (5), 38−51.

(13) Lodahl, P.; Mahmoodian, S.; Stobbe, S. Interfacing single photons and single quantum dots with photonic nanostructures. *Rev. Mod. Phys.* **2015**, *87* (2), 347.

(14) Wang, H.; Hu, H.; Chung, T.-H.; Qin, J.; Yang, X.; Li, J.-P.; Liu, R.-Z.; Zhong, H.-S.; He, Y.-M.; Ding, X. On-demand semiconductor source of entangled photons which simultaneously has high fidelity, efficiency, and indistinguishability. *Physical review letters* **2019**, *122* (11), 113602.

(15) Tomm, N.; Javadi, A.; Antoniadis, N. O.; Najer, D.; Lobl, M. C.; Korsch, A. R.; Schott, R.; Valentin, S. R.; Wieck, A. D.; Ludwig, A.; Warburton, R. J. A bright and fast source of coherent single photons. *Nat. Nanotechnol* **2021**, *16* (4), 399−403.

(16) Huber, D.; Reindl, M.; Huo, Y.; Huang, H.; Wildmann, J. S.; Schmidt, O. G.; Rastelli, A.; Trotta, R. Highly indistinguishable and strongly entangled photons from symmetric GaAs quantum dots. *Nat. Commun.* **2017**, *8* (1), 15506.

(17) Appel, M. H.; Tiranov, A.; Pabst, S.; Chan, M. L.; Starup, C.; Wang, Y.; Midolo, L.; Tiurev, K.; Scholz, S.; Wieck, A. D. Entangling a hole spin with a time-bin photon: a waveguide approach for quantum dot sources of multiphoton entanglement. *Phys. Rev. Lett.* **2022**, *128* (23), 233602.

(18) Lodahl, P.; Floris Van Driel, A.; Nikolaev, I. S.; Irman, A.; Overgaag, K.; Vanmaekelbergh, D.; Vos, W. L. Controlling the dynamics of spontaneous emission from quantum dots by photonic crystals. *Nature* **2004**, *430* (7000), 654−657 (acccessed 2020−01−24 01:07:02).DOI.org (Crossref).

(19) Moody, G.; Sorger, V. J.; Blumenthal, D. J.; Juodawlkis, P. W.; Loh, W.; Sorace-Agaskar, C.; Jones, A. E.; Balram, K. C.; Matthews, J. C.; Laing, A. 2022 Roadmap on integrated quantum photonics. *Journal of Physics: Photonics* **2022**, *4* (1), 012501.

(20) Wang, J.; Sciarrino, F.; Laing, A.; Thompson, M. G. Integrated photonic quantum technologies. *Nat. Photonics* **2020**, *14* (5), 273−284.

(21) Arakawa, Y.; Holmes, M. J. Progress in quantum-dot single photon sources for quantum information technologies: A broad spectrum overview. *Applied Physics Reviews* **2020**, *7* (2), 021309.

(22) García de Arquer, F. P.; Talapin, D. V.; Klimov, V. I.; Arakawa, Y.; Bayer, M.; Sargent, E. H. Semiconductor quantum dots: Technological progress and future challenges. *Science* **2021**, *373* (6555), No. eaaz8541.

(23) Schimpf, C.; Reindl, M.; Basso Basset, F.; Jöns, K. D.; Trotta, R.; Rastelli, A. Quantum dots as potential sources of strongly entangled photons: Perspectives and challenges for applications in quantum networks. *Appl. Phys. Lett.* **2021**, *118* (10), 100502.

(24) Gurioli, M.; Wang, Z.; Rastelli, A.; Kuroda, T.; Sanguinetti, S. Droplet epitaxy of semiconductor nanostructures for quantum photonic devices. *Nat. Mater.* **2019**, *18* (8), 799−810.

(25) Watanabe, K.; Koguchi, N.; Gotoh, Y. Fabrication of GaAs quantum dots by modified droplet epitaxy. *Jpn. J. Appl. Phys.* **2000**, *39* (2A), L79.

(26) da Silva, S. F. C.; Undeutsch, G.; Lehner, B.; Manna, S.; Krieger, T. M.; Reindl, M.; Schimpf, C.; Trotta, R.; Rastelli, A. GaAs

https://doi.org/10.1021/acs.nanolett.3c04846
Nano Lett. XXXX, XXX, XXX−XXX

quantum dots grown by droplet etching epitaxy as quantum light sources. *Appl. Phys. Lett.* **2021**, *119*, 120502.
(27) Zhai, L.; Löbl, M. C.; Nguyen, G. N.; Ritzmann, J.; Javadi, A.; Spinnler, C.; Wieck, A. D.; Ludwig, A.; Warburton, R. J. Low-noise GaAs quantum dots for quantum photonics. *Nat. Commun.* **2020**, *11* (1), 4745.
(28) Zhai, L.; Nguyen, G. N.; Spinnler, C.; Ritzmann, J.; Löbl, M. C.; Wieck, A. D.; Ludwig, A.; Javadi, A.; Warburton, R. J. Quantum interference of identical photons from remote GaAs quantum dots. *Nat. Nanotechnol* **2022**, *17* (8), 829−833.
(29) Basso Basset, F.; Valeri, M.; Roccia, E.; Muredda, V.; Poderini, D.; Neuwirth, J.; Spagnolo, N.; Rota, M. B.; Carvacho, G.; Sciarrino, F.; Trotta, R. Quantum key distribution with entangled photons generated on demand by a quantum dot. *Science advances* **2021**, *7* (12), No. eabe6379.
(30) Huber, D.; Reindl, M.; da Silva, S. F. C.; Schimpf, C.; Martín-Sánchez, J.; Huang, H.; Piredda, G.; Edlinger, J.; Rastelli, A.; Trotta, R. Strain-tunable GaAs quantum dot: A nearly dephasing-free source of entangled photon pairs on demand. *Physical review letters* **2018**, *121* (3), 033902.
(31) Sapienza, L.; Davanço, M.; Badolato, A.; Srinivasan, K. Nanoscale optical positioning of single quantum dots for bright and pure single-photon emission. *Nat. Commun.* **2015**, *6* (1), 7833.
(32) Wang, H.; He, Y.-M.; Chung, T.-H.; Hu, H.; Yu, Y.; Chen, S.; Ding, X.; Chen, M.-C.; Qin, J.; Yang, X. Towards optimal single-photon sources from polarized microcavities. *Nat. Photonics* **2019**, *13* (11), 770−775.
(33) Tiranov, A.; Angelopoulou, V.; van Diepen, C. J.; Schrinski, B.; Sandberg, O. A. D. A.; Wang, Y.; Midolo, L.; Scholz, S.; Wieck, A. D.; Ludwig, A. Collective super-and subradiant dynamics between distant optical quantum emitters. *Science* **2023**, *379* (6630), 389−393.
(34) Lukin, D. M.; Guidry, M. A.; Yang, J.; Ghezellou, M.; Mishra, S. D.; Abe, H.; Ohshima, T.; Ul-Hassan, J.; Vučković, J. Two-Emitter Multimode Cavity Quantum Electrodynamics in Thin-Film Silicon Carbide Photonics. *Physical Review X* **2023**, *13* (1), 011005.
(35) Liu, S.; Srinivasan, K.; Liu, J. Nanoscale positioning approaches for integrating single solid-state quantum emitters with photonic nanostructures. *Laser & Photonics Reviews* **2021**, *15* (10), 2100223.
(36) Redjem, W.; Zhiyenbayev, Y.; Qarony, W.; Ivanov, V.; Papapanos, C.; Liu, W.; Jhuria, K.; Al Balushi, Z.; Dhuey, S.; Schwartzberg, A. All-silicon quantum light source by embedding an atomic emissive center in a nanophotonic cavity. *Nat. Commun.* **2023**, *14* (1), 3321.
(37) Han, I. S.; Wang, Y.-R.; Hopkinson, M. Ordered GaAs quantum dots by droplet epitaxy using in situ direct laser interference patterning. *Appl. Phys. Lett.* **2021**, *118*, 142101.
(38) Surrente, A.; Felici, M.; Gallo, P.; Rudra, A.; Dwir, B.; Kapon, E. Dense arrays of site-controlled quantum dots with tailored emission wavelength: Growth mechanisms and optical properties. *Appl. Phys. Lett.* **2017**, *111*, 221102.
(39) Felici, M.; Gallo, P.; Mohan, A.; Dwir, B.; Rudra, A.; Kapon, E. Site-Controlled InGaAs Quantum Dots with Tunable Emission Energy. *Small* **2009**, *5* (8), 938−943.
(40) Zhang, J.; Chattaraj, S.; Huang, Q.; Jordao, L.; Lu, S.; Madhukar, A. On-chip scalable highly pure and indistinguishable single-photon sources in ordered arrays: path to quantum optical circuits. *Science Advances* **2022**, *8* (35), No. eabn9252.
(41) Yakes, M. K.; Yang, L.; Bracker, A. S.; Sweeney, T. M.; Brereton, P. G.; Kim, M.; Kim, C. S.; Vora, P. M.; Park, D.; Carter, S. G.; Gammon, D. Leveraging crystal anisotropy for deterministic growth of InAs quantum dots with narrow optical linewidths. *Nano Lett.* **2013**, *13* (10), 4870−4875.
(42) Wang, L.; Rastelli, A.; Kiravittaya, S.; Atkinson, P.; Ding, F.; Bufon, C. B.; Hermannstädter, C.; Witzany, M.; Beirne, G.; Michler, P. Towards deterministically controlled InGaAs/GaAs lateral quantum dot molecules. *New J. Phys.* **2008**, *10* (4), 045010.
(43) Schnauber, P.; Schall, J.; Bounouar, S.; Hohne, T.; Park, S.-I.; Ryu, G.-H.; Heindel, T.; Burger, S.; Song, J.-D.; Rodt, S.; Reitzenstein, S. Deterministic integration of quantum dots into on-chip multimode interference beamsplitters using in situ electron beam lithography. *Nano Lett.* **2018**, *18* (4), 2336−2342.
(44) Schneider, C.; Heindel, T.; Huggenberger, A.; Weinmann, P.; Kistner, C.; Kamp, M.; Reitzenstein, S.; Höfling, S.; Forchel, A. Single photon emission from a site-controlled quantum dot-micropillar cavity system. *Applied physics letters* **2009**, *94*, 111111.
(45) Prieto, I.; Herranz, J.; González, Y.; Canet-Ferrer, J.; Wewior, L.; Postigo, P.; Alén, B.; González, L.; Kaldirim, M.; Munioz-Camuniez, L. Different strategies towards the deterministic coupling of a single quantum dot to a photonic crystal cavity mode. In *2011 13th International Conference on Transparent Optical Networks*, 2011; IEEE: pp 1−5.
(46) Badolato, A.; Hennessy, K.; Atature, M.; Dreiser, J.; Hu, E.; Petroff, P. M.; Imamoglu, A. Deterministic coupling of single quantum dots to single nanocavity modes. *Science* **2005**, *308* (5725), 1158−1161.
(47) Iyer, P. P.; Karl, N.; Addamane, S.; Gennaro, S. D.; Sinclair, M. B.; Brener, I. Sub-picosecond steering of ultrafast incoherent emission from semiconductor metasurfaces. *Nat. Photonics* **2023**, *17*, 588−593.
(48) Tian, J.; Adamo, G.; Liu, H.; Klein, M.; Han, S.; Liu, H.; Soci, C. Optical rashba effect in a light-emitting perovskite metasurface. *Adv. Mater.* **2022**, *34* (12), 2109157.
(49) Iyer, P. P.; DeCrescent, R. A.; Mohtashami, Y.; Lheureux, G.; Butakov, N. A.; Alhassan, A.; Weisbuch, C.; Nakamura, S.; DenBaars, S. P.; Schuller, J. A. Unidirectional luminescence from InGaN/GaN quantum-well metasurfaces. *Nat. Photonics* **2020**, *14* (9), 543−548.
(50) Khoury, M.; Quard, H.; Herzig, T.; Meijer, J.; Pezzagna, S.; Cueff, S.; Abbarchi, M.; Nguyen, H. S.; Chauvin, N.; Wood, T. Light Emitting Si-Based Mie Resonators: Toward a Huygens Source of Quantum Emitters. *Advanced Optical Materials* **2022**, *10* (21), 2201295.
(51) Liu, S.; Vaskin, A.; Addamane, S.; Leung, B.; Tsai, M.-C.; Yang, Y.; Vabishchevich, P. P.; Keeler, G. A.; Wang, G.; He, X. Light-emitting metasurfaces: simultaneous control of spontaneous emission and far-field radiation. *Nano Lett.* **2018**, *18* (11), 6906−6914.
(52) Schimpf, C.; Reindl, M.; Huber, D.; Lehner, B.; Covre Da Silva, S. F.; Manna, S.; Vyvlecka, M.; Walther, P.; Rastelli, A. Quantum cryptography with highly entangled photons from semiconductor quantum dots. *Science advances* **2021**, *7* (16), No. eabe8905.
(53) Flamini, F.; Spagnolo, N.; Sciarrino, F. Photonic quantum information processing: a review. *Rep. Prog. Phys.* **2019**, *82* (1), 016001.
(54) Madsen, L. S.; Laudenbach, F.; Askarani, M. F.; Rortais, F.; Vincent, T.; Bulmer, J. F.; Miatto, F. M.; Neuhaus, L.; Helt, L. G.; Collins, M. J. Quantum computational advantage with a programmable photonic processor. *Nature* **2022**, *606* (7912), 75−81.
(55) Decker, M.; Staude, I.; Falkner, M.; Dominguez, J.; Neshev, D. N.; Brener, I.; Pertsch, T.; Kivshar, Y. S. High-efficiency dielectric Huygens' surfaces. *Advanced Optical Materials* **2015**, *3* (6), 813−820.
(56) Iyer, P. P.; Butakov, N. A.; Schuller, J. A. Reconfigurable Semiconductor Phased-Array Metasurfaces. *ACS Photonics* **2015**, *2* (8), 1077−1084 (acccessed 2020-01-24 01:07:02).DOI.org (Crossref).
(57) Lourenço, S.; Dias, I.; Duarte, J.; Laureto, E.; Meneses, E.; Leite, J.; Mazzaro, I. Temperature dependence of optical transitions in AlGaAs. *J. Appl. Phys.* **2001**, *89* (11), 6159−6164.
(58) Kokubo, Y.; Ohta, I. Refractive index as a function of photon energy for AlGaAs between 1.2 and 1.8 eV. *Journal of applied physics* **1997**, *81* (4), 2042−2043.
(59) Abbarchi, M.; Troiani, F.; Mastrandrea, C.; Goldoni, G.; Kuroda, T.; Mano, T.; Sakoda, K.; Koguchi, N.; Sanguinetti, S.; Vinattieri, A.; Gurioli, M. Spectral diffusion and line broadening in single self-assembled GaAs/AlGaAs quantum dot photoluminescence. *Applied physics letters* **2008**, *93*, 162101.
(60) Basso Basset, F.; Bietti, S.; Tuktamyshev, A.; Vichi, S.; Bonera, E.; Sanguinetti, S. Spectral broadening in self-assembled GaAs quantum dots with narrow size distribution. *J. Appl. Phys.* **2019**, *126*, 024301.

https://doi.org/10.1021/acs.nanolett.3c04846
Nano Lett. XXXX, XXX, XXX−XXX

(61) Rakhlin, M.; Belyaev, K.; Klimko, G.; Mukhin, I.; Kirilenko, D.; Shubina, T.; Ivanov, S.; Toropov, A. InAs/AlGaAs quantum dots for single-photon emission in a red spectral range. *Sci. Rep.* **2018**, *8* (1), 5299.
(62) Zhou, T.; Tang, M.; Xiang, G.; Xiang, B.; Hark, S.; Martin, M.; Baron, T.; Pan, S.; Park, J.-S.; Liu, Z. Continuous-wave quantum dot photonic crystal lasers grown on on-axis Si (001). *Nat. Commun.* **2020**, *11* (1), 977.
(63) Gao, K.; Holmes, M.; Arita, M.; Arakawa, Y. Measurement of the emission lifetime of a GaN interface fluctuation quantum dot by power dependent single photon dynamics. *physica status solidi (a)* **2018**, *215* (9), 1700630.
(64) Becher, C.; Kiraz, A.; Michler, P.; Imamoğlu, A.; Schoenfeld, W.; Petroff, P.; Zhang, L.; Hu, E. Nonclassical radiation from a single self-assembled InAs quantum dot. *Phys. Rev. B* **2001**, *63* (12), 121312.
(65) Beveratos, A.; Brouri, R.; Gacoin, T.; Poizat, J.-P.; Grangier, P. Nonclassical radiation from diamond nanocrystals. *Phys. Rev. A* **2001**, *64* (6), 061802.
(66) Heyn, C.; Strelow, C.; Hansen, W. Excitonic lifetimes in single GaAs quantum dots fabricated by local droplet etching. *New J. Phys.* **2012**, *14* (5), 053004.
(67) Abbarchi, M.; Gurioli, M.; Sanguinetti, S.; Zamfirescu, M.; Vinattieri, A.; Koguchi, N. Recombination lifetime of single GaAs/AlGaAs quantum dots. *physica status solidi c* **2006**, *3* (11), 3860−3863.
(68) Schöll, E.; Hanschke, L.; Schweickert, L.; Zeuner, K. D.; Reindl, M.; Covre da Silva, S. F.; Lettner, T.; Trotta, R.; Finley, J. J.; Müller, K. Resonance fluorescence of GaAs quantum dots with near-unity photon indistinguishability. *Nano Lett.* **2019**, *19* (4), 2404−2410.
(69) Noda, S.; Fujita, M.; Asano, T. Spontaneous-emission control by photonic crystals and nanocavities. *Nat. Photonics* **2007**, *1* (8), 449−458 (acccessed 2020-01-24 01:07:02).DOI.org (Crossref).

https://doi.org/10.1021/acs.nanolett.3c04846
Nano Lett. XXXX, XXX, XXX−XXX